Experimental Astronomy (2025) 60:21
https://doi.org/10.1007/s10686-025-10029-5

RESEARCH

Characterization of a half wave plate and a polarizer for accurate starlight polarimetry

Paolo de Bernardis[1,2,3] · **Silvia Masi**[1,2,3] · **Giulia Barbieri Ripamonti**[1,3] · **Fabio Columbro**[1,3]

Received: 7 May 2025 / Accepted: 9 September 2025

Abstract
In the process of developing a space-based imaging Stokes polarimeter for starlight polarization measurements, we established a procedure to characterize its two main optical components: the wave plate and the polarizer. We demonstrate that a simple optical bench setup combined with a custom calibration procedure can be used to measure the non-ideality parameters of both the polarizer and the wave plate. Using this approach, we characterized two high-quality components for the V-band. We set an upper limit for the cross-polarization of the polarizer, $C_B \leq 1 \times 10^{-4}$, and a limit of $\Delta \leq 2 \times 10^{-4}$ for the transmission imbalance of the half-wave plate. We show that with these components the setup yields reproducible measurements at the level of 0.001% for the polarization degree of a weakly polarized source, and $3'$ for the position angle. We also investigate the performance of the components under tilted incidence, up to 6^o off-axis, as required for a wide-field imaging version of a stellar polarimeter. We find that within this range, even without any off-axis bias correction, these components enable measurements of the polarization degree with an accuracy better than 0.005, and of the polarization angle with an accuracy better than 1^o.

Keywords Polarimetry · Starlight polarization

1 Introduction

The measurement of starlight polarization (see [1–3], and [4] for a review) is a powerful tool to study interstellar dust grains and their distribution, as well as the magnetic field of our Galaxy (see e.g. [5] and references therein). Moreover, surveys of starlight polarization are complementary to measurements of the polarization of the Cosmic Microwave Background (CMB, see e.g. [6]).

Extended author information available on the last page of the article

Published online: 28 October 2025

A Stokes polarimeter [7, 8], consisting of a rotating half-wave plate (HWP) followed by a linear polarizer (analyzer) and a power detector, can be used to measure low levels of linear polarization, especially if the HWP is the first optical element skyward (see e.g. [9, 10]). In such an instrument, the linearly polarized component of the brightness is modulated at four times the rotation frequency of the HWP ($4f$).

The availability of sensitive CCD cameras for visible wavelengths motivates the development of an imaging version of the Stokes polarimeter, using sufficiently large optical components (HWP and analyzer) as the first elements in the optical system. Such an instrument would be well suited for accurate sky surveys of stellar polarization.These surveys (see e.g. [11–13] and references therein) are usually limited by photon noise and atmospheric effects, such as seeing. However, in a space-based implementation of a stellar polarimeter, where stellar fields can be observed for long periods and atmospheric effects are absent, the main limitation becomes the level of systematic effects produced in the instrument (see e.g. [14]). This motivated the study presented here.

Real HWPs and polarizers for the optical band suffer from a number of non-idealities that affect the performance of the polarimeter (see e.g. [15–18]). As we show in the theory section, the main systematic effect due to non-idealities in the HWP and the polarizer in our application is a modulation of the unpolarized brightness at twice the rotation frequency ($2f$). This may challenge the dynamic range of the detector in systems designed to measure very small polarization degrees. For this reason, it is important to optimize the optical components to minimize their non-idealities and to characterize their performance with high accuracy.

To this end, we set up an optical bench to characterize the performance of large (~ 10 cm diameter) HWPs and polarizers for the visual band. For our instrument we selected high-performance devices with the specifications reported in Table 1.

In the following Sections 2 and 3, we show that our setup can detect transmission imbalance in the HWP and cross-polarization in the polarizer at sub-percent levels. For the components we analyzed, we provide stringent upper limits on these parameters, demonstrating that they enable measurements of the polarization degree with an accuracy better than 0.1%, and of the polarization angle with an accuracy of $\sim 1^o$.

Table 1 Specifications for the optical devices (polarizer and HWP) used in this study

Polarizer	
clear aperture	$\geq$ 90 mm
nominal operating wavelength range	Johnson's V-band
contrast ratio	$>$ 1000 throughout V-band
beam deviation	$\leq 1'$
TWD (P-V at 632.8nm)	$\leq \lambda/4$ per inch
HWP	
clear aperture	$\geq$ 90 mm
nominal operating wavelength range	Johnson's V-band
maximum retardance deviation from 0.5λ	$< 2\%$ throughout V-band
beam deviation	$\leq 2'$
TWD (P-V at 632.8nm)	$\leq 1\lambda$ per inch

In Section 4, we use the same setup to analyze the response of the Stokes polarimeter, composed of the HWP and polarizer, to obliquely incident rays.

2 Characterization of the polarizer

In order to characterize the transmission of the analyzer polarizer, we illuminate it using a polarized source and measure the power received from a power detector placed behind the analyzer, when the analyzer is rotated around the optical axis.

2.1 Theory

The power detected by a detector that is not sensitive to polarization, receiving radiation from a generic source through a non-ideal analyzer polarizer (a diattenuator) is (see e.g. [19]):

$$W_\gamma = [1 \quad 0 \quad 0 \quad 0] \times \mathcal{D}_{\gamma,A} \times \begin{bmatrix} \mathrm{I} \\ \mathrm{Q} \\ \mathrm{U} \\ \mathrm{V} \end{bmatrix} \tag{1}$$

where I, Q, U, V are the Stokes parameters of the source, and

$$\mathcal{D}_{\gamma,A} = \frac{1}{2} \begin{bmatrix} P_A & c_{2\gamma}\Delta_A & s_{2\gamma}\Delta_A & 0 \\ c_{2\gamma}\Delta_A & c_{2\gamma}^2 P_A + s_{2\gamma}^2 X_A & c_{2\gamma}s_{2\gamma}(P_A - X_A) & 0 \\ s_{2\gamma}\Delta_A & c_{2\gamma}s_{2\gamma}(P_A - X_A) & s_{2\gamma}^2 P_A + c_{2\gamma}^2 X_A & 0 \\ 0 & 0 & 0 & X_A \end{bmatrix} \tag{2}$$

is the Mueller matrix of the analyzer diattenuator A, in a reference system where z is the propagation axis and the x and y axes are on the wavefront plane. Here, the polarizer is rotated by γ with respect to the x axis, with $c_{2\gamma} = \cos 2\gamma$, $s_{2\gamma} = \sin 2\gamma$, and, if $p_{A,x}$ and $p_{A,y}$ are the transmissions for the electrical field components along the main axis of the polarizer and along the orthogonal axis, it is $P_A = p_{A,x}^2 + p_{A,y}^2$, $\Delta_A = p_{A,x}^2 - p_{A,y}^2$, $X_A = 2p_{A,x}p_{A,y}$. For an ideal polarizer, $P_A = 1$, $|\Delta_A| = 1$, $X_A = 0$. The deviation from these ideal values quantify the non-ideality of the polarizer. Another way to quantify the non-ideality of the polarizer is to estimate the efficiency of the polarizer $E_A = \sqrt{P_A}$ and its cross-polarization C_A, defined as

$$C_A = \frac{p_{A,y}^2}{p_{A,x}^2}. \tag{3}$$

so that

$$C_A = \frac{1 - \Delta_A/P_A}{1 + \Delta_A/P_A}. \tag{4}$$

Here we consider a case with no circular polarization of the source (V = 0), so we have

$$W_\gamma = \frac{1}{2}[P_A \mathrm{I} + c_{2\gamma}\Delta_A \mathrm{Q} + s_{2\gamma}\Delta_A \mathrm{U}] \tag{5}$$

If the source is totally polarized with the electric vector oriented at an angle α with respect to the *x* axis, we have

$$W_\gamma = \frac{\mathrm{I}}{2}[P_A + (c_{2\gamma}c_{2\alpha} + s_{2\gamma}s_{2\alpha})\Delta_A] \tag{6}$$

i.e.

$$W_\gamma = \frac{\mathrm{I}}{2}\big[P_A + \Delta_A \cos[2(\alpha - \gamma)]\big] \tag{7}$$

In a measurement changing the rotation angle of the polarizer γ while the orientation of the source α remains constant, one measures (Malus law)

$$\frac{W_\gamma}{W_{max}} = \frac{1 + a\cos[2(\alpha - \gamma)]}{1 + a} \tag{8}$$

where

$$a = \frac{\Delta_A}{P_A} = \frac{p_{A,x}^2 - p_{A,y}^2}{p_{A,x}^2 + p_{A,y}^2} = \frac{1 - C_A}{1 + C_A}. \tag{9}$$

Note that

$$C_A = \frac{1 - a}{1 + a} = min\left[\frac{W_\gamma}{W_{max}}\right] = m \tag{10}$$

so the minimum of the measured normalized data provides an estimate for C_A.

In the case of a partially polarized source, described by the Stokes vector

$$\begin{bmatrix} \mathrm{I} \\ \mathrm{Q} \\ \mathrm{U} \\ \mathrm{V} \end{bmatrix} = \mathrm{I} \begin{bmatrix} 1 \\ pc_{2\alpha} \\ ps_{2\alpha} \\ 0 \end{bmatrix} \tag{11}$$

where $0 \le p \le 1$ is the polarization degree of the source, we have a detected power

$$W_{\beta,\gamma} = \frac{\mathrm{I}}{2}\big[P_A + p\Delta_A \cos[2(\alpha - \gamma)]\big] \tag{12}$$

or

$$\frac{W_\gamma}{W_{max}} = \frac{1 + b\cos[2(\alpha - \gamma)]}{1 + b} \tag{13}$$

where

$$b = p\frac{\Delta_A}{P_A} = p\frac{p_{A,x}^2 - p_{A,y}^2}{p_{A,x}^2 + p_{A,y}^2} = p\frac{1 - C_A}{1 + C_A} \tag{14}$$

and also

$$C_A = \frac{1 - b/p}{1 + b/p}. \tag{15}$$

This means that this measurement alone cannot separate the effect of the polarization degree of the source from the effect of the cross-polarization of the polarizer. In Fig. 1 we show the cross-polarization implied by a measured value of b close to 1, for different values of the polarization degree of the source, all close to 1.

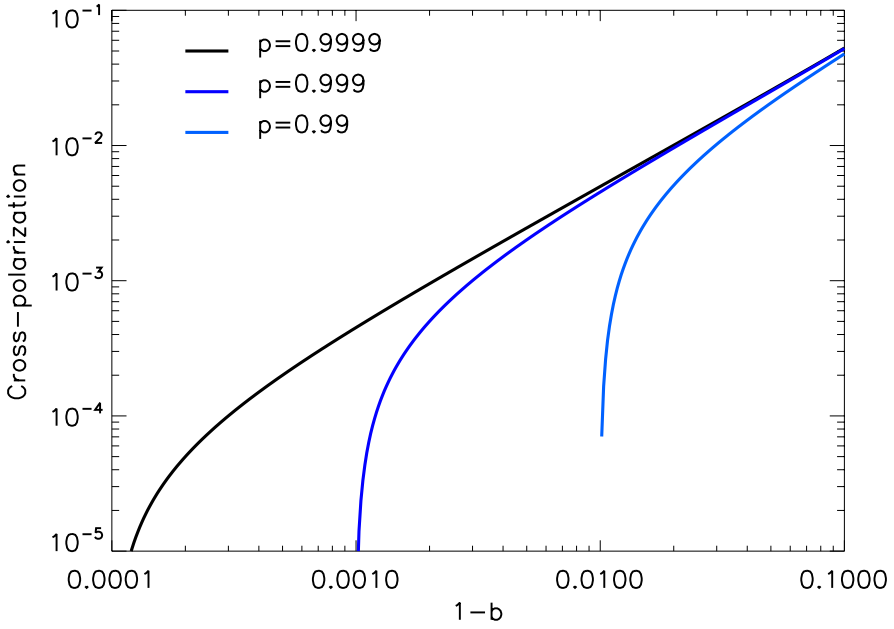

Fig. 1 Cross-polarization implied by a measured value of b close to 1, for different values of the polarization degree p of the source, all close to 1

Let's call again *m* the minimum value of the measured and normalized signal. Here

$$m = min\left[\frac{W_\gamma}{W_{max}}\right] = \frac{1-b}{1+b} \tag{16}$$

Combining with (15) we find

$$C_A = \frac{m(1+p)-(1-p)}{(1+p)-m(1-p)}. \tag{17}$$

Only if the polarization degree *p* is very close to 1, such that $m(1+p) \gg (1-p)$, then we can approximate

$$C_A \simeq m\left[1+\frac{m(1-p)}{2}\right] \simeq m. \tag{18}$$

Roughly speaking, to obtain an univocal determination of C_A from the measurement, the difference between the polarization degree of the source and 1 should be much less than the value of C_A. Only under this condition, the measured *m* is an estimate of the cross-polarization C_A. Otherwise, *m* will be an upper limit for the value of C_A. So, in order to measure low-levels of cross-polarization, one has to use a beam with high polarization degree.

If the source itself is not intrinsically polarization-pure, we can use a first polarizer *B* as a *purifying* polarizer, and insert the polarizer *A* under test between *B* and the detector. *B* has Mueller matrix $\mathcal{D}_{\gamma,B}$, while the polarizer under test *A* will have Mueller matrix $\mathcal{D}_{\beta,A}$. The signal on the detector in this case will be

$$W_{\beta,\gamma} = [1 \quad 0 \quad 0 \quad 0] \times \mathcal{D}_{\beta,A} \times \mathcal{D}_{\gamma,B} \times \begin{bmatrix} \mathrm{I} \\ \mathrm{Q} \\ \mathrm{U} \\ \mathrm{V} \end{bmatrix} \tag{19}$$

so that

$$\begin{aligned} W_{\beta,\gamma} = \frac{\mathrm{I}}{4}\Big[& P_A P_B + \Delta_A \Delta_B (c_{2\beta}c_{2\gamma} + s_{2\beta}s_{2\gamma}) + \\ & + P_A (c_{2\alpha}c_{2\gamma} + s_{2\alpha}s_{2\gamma})\Delta_B p + \\ & + (c_{2\alpha}c_{2\beta} + s_{2\alpha}s_{2\beta})(c_{2\gamma}^2 P_B + s_{2\gamma}^2 X_B)\Delta_A p + \\ & + (s_{2\alpha}c_{2\beta} + c_{2\alpha}s_{2\beta})c_{2\gamma}s_{2\gamma}(P_B - X_B)\Delta_A p \Big] \end{aligned} \tag{20}$$

i.e.

$$W_{\beta,\gamma} = \frac{\mathrm{I}}{4}\Big[P_A P_B + c_{2(\beta-\gamma)}\Delta_A\Delta_B + \\ + c_{2(\alpha-\gamma)}P_A\Delta_B p + \\ + c_{2(\beta-\gamma)}c_{2(\alpha-\gamma)}\Delta_A P_B p + \\ + s_{2(\beta-\gamma)}s_{2(\alpha-\gamma)}\Delta_A X_B p\Big] \tag{21}$$

If we align the main axis of the purifying polarizer B to the direction of polarization of the source, i.e. if we have $\gamma = \alpha$, then

$$W_{\beta,\gamma} = \frac{\mathrm{I}}{4}\big[P_A(P_B + \Delta_B p) + c_{2(\beta-\gamma)}\Delta_A(\Delta_B + P_B p)\big] \tag{22}$$

In this configuration,

$$\frac{W_{\beta,\gamma}}{W_{max}} = \frac{P_A(P_B + \Delta_B p) + c_{2(\beta-\gamma)}\Delta_A(\Delta_B + P_B p)}{P_A(P_B + \Delta_B p) + \Delta_A(\Delta_B + P_B p)} \tag{23}$$

or

$$\frac{W_{\beta,\gamma}}{W_{max}} = \frac{1 + b' c_{2(\beta-\gamma)}}{1 + b'} \tag{24}$$

where

$$b' = \frac{\Delta_A}{P_A} \cdot \frac{\Delta_B + pP_B}{P_B + p\Delta_B} \tag{25}$$

Comparing to (14), we see that this is equivalent to carrying out a measurement of the polarizer under test A using a source with polarization degree

$$p' = \frac{\Delta_B + pP_B}{P_B + p\Delta_B} \tag{26}$$

which is larger than p. If, for example, $p = 0.9$ and $C_B = 0.05$, we have already $p' = 0.995$; if $p = 0.95$ and $C_B = 0.01$, we have $p' = 0.9995$. As expected, adding a polarizer with its main axis aligned to the source polarization axis purifies the linear polarization of the beam, thus allowing the measurement of small levels of cross-polarization in the devices illuminated by the source.

2.2 Polarizer measurements

2.2.1 Preliminary measurement

The two components we have selected (Table 1) are optimized for the V-band of the Johnson system. If we remain within the limits of this band, chromatic effects typical of generic HWP and polarizers (see e.g.[20–22]) are expected to be negligible. For this reason the measurements are obtained with a setup including either a green laser diode (model OSRAM PLT3 520FB, λ = 520 nm, nominal polarization ratio $> 50:1$) or a commercial green LED (Kingbright L53-GD, λ = 565 nm, nominally unpolarized) as sources. The setup is completed by a commercial photo-camera polarizer (Hama Pol Linear M49) on a rotary stage (to further purify the polarization state of the laser diode), a lens, a photodiode (model BPW21R from Vishay). Both the LED and the laser diode source are modulated at 210 Hz, and the measured signal is the result of synchronous demodulation obtained with a lock-in amplifier (model MFLI from Zurich Instruments). In this way no correction for dark current is required, and dark current variations do not affect our results since they are negligible at the modulation frequency.

The optical setup is sketched in Fig. 2.

The distance between the source and the lens is 1.5 m, and the used diameter of the lens is 4 cm, so that the maximum off-axis incidence angle at the HWP is of the order of 0.75°. We have used the formalism described in [23] (see Appendix A) to estimate the modulation of the HWP for slightly slant rays contributing to the beam considered here. Averaging over uniformly weighted rays filling a 1.5^o FWHM beam, we find

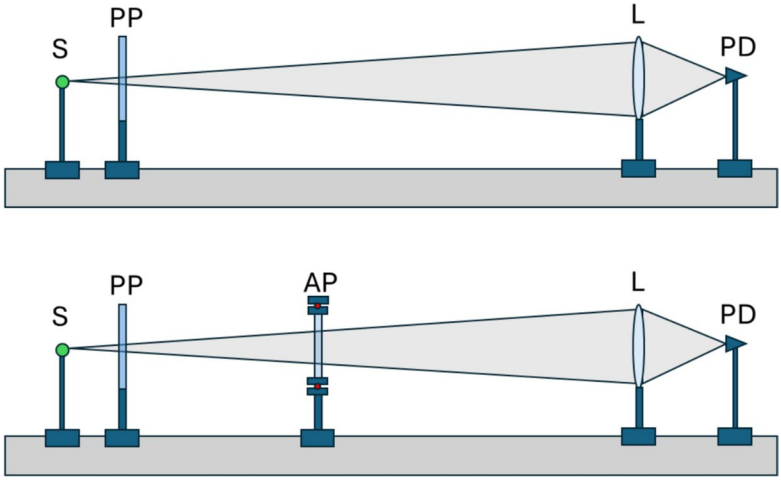

Fig. 2 **Top:** Measurement setup for the preliminary measurement. **Bottom:** measurement setup for the characterization of the analyzer polarizer. From left to right: laser diode source (S), purifying polarizer (PP), analyzer polarizer with its rotary stage (AP), lens (L), photodetector (PD)

that, during the rotation of the HWP, the maximum deviation of the detected signal from the one expected for a parallel beam is $< 0.3\%$. This implies an even smaller bias in the determination of the polarization degree of the source (-0.05%), and a totally negligible variation of the estimate of its polarization angle. We conclude that the modulation properties are not significantly affected by the mild beam divergence used in our setup.

A precision rotation stage is used to step the analyzer polarizer (Section 2.2.2) or the HWP (Section 3.2) in 11.25° steps, with a positioning error $< 1'$. We measure a number of orientations larger than the minimum of four normally used for polarimetry, since in this calibration process we search for small systematic effects which can produce a polarimetric response with angular dependence deviating from the standard. Oversampling the orientation angles helps to distinguish the different components of the detected signal, like those depending on $n\gamma$ (see Section 3.1.2), possible drifts due to source intensity variations, and the effects of small misalignments.

The stability of the system has been tested with the setup sketched in the top panel of Fig. 2, by acquiring the detected signal under steady conditions (constant amplitude and frequency of the laser diode current, constant angles θ and γ).

We verify that over a timescale of a few minutes (such as the one required to measure the Malus law) the system is stable to better than 1 part over 1000. Then, still with the laser diode source and the setup of the top panel of Fig. 2, we measure the demodulated output for different orientations of the purifying polarizer, obtaining the data reported in Fig. 3(black diamonds).

The minimum of the normalized signal is $m \sim 3.5\%$, which, as we have seen, represents an upper limit for the cross-polarization C_B of the commercial photocamera polarizer.

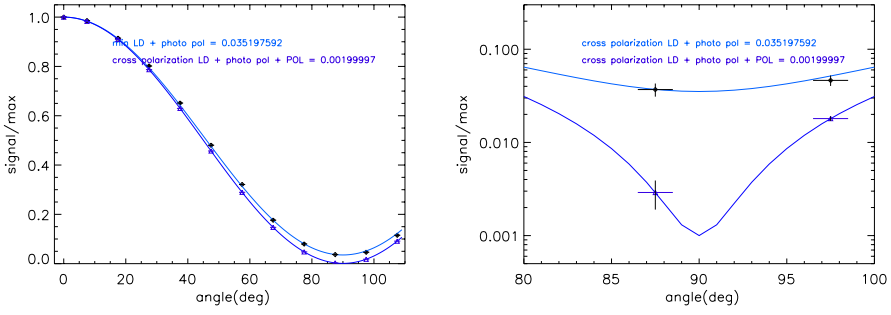

Fig. 3 **Left:** The diamonds with error bars represent the measurements of the normalized detected power through a commercial polarizer for photo cameras for the configuration sketched in the top panel of Fig. 2; the best fit of the data is obtained with (13). The triangles with error bars represent the measurements of the normalized detected power when the analyzer polarizer is illuminated by the same source, through the commercial polarizer used as a purifying polarizer (configuration sketched in the bottom panel of Fig. 2). **Right:** zoom of the same data in the region of minimum transmitted signal. The cross-polarizations are estimated from the minima using (18).

2.2.2 Test of the analyzer polarizer

We then orient the purifying polarizer with its main axis parallel to the polarization direction of the source. We introduce a high quality analyzer polarizer (model VFM-119mm-UV from Meadowlark Optics - see Table 1) between the purifying polarizer and the lens, and record the detected power as a function of the angle $\beta - \gamma$ (see left panel of Fig. 3).

The minimum demodulated signal from the photodiode, normalized to the maximum, is 2×10^{-4}, and the minimum of the best fit, for $\beta = \gamma + \pi/2$ is 1×10^{-4}, so

$$m = min\left[\frac{W_\beta}{W_{max}}\right] = 1 \times 10^{-4} \tag{27}$$

Using (18) and our estimated values for m and P' we conclude that the cross-polarization of this analyzer polarizer is

$$C_A \leq 1 \times 10^{-4} \tag{28}$$

The efficiency P_A is estimated from the ratio R of the signal with the analyzer polarizer and the signal without the analyzer polarizer, when $\beta = \gamma$. Using the unpolarized LED diode we get $R = (0.865 \pm 0.002)$. From (22), in this case we have $R = (1 + C_A C_B) p_{A,x}^2 \simeq p_{A,x}^2$ since C_A and C_B are both $\ll 1$, and thus $P_A \simeq \Delta_A \simeq (0.865 \pm 0.002)$.

3 Characterization of the HWP

3.1 Theory

3.1.1 HWP model

We model the Mueller matrix of the real HWP as the product of an ideal retarder matrix $\mathcal{R}$, times a diattenuator matrix $\mathcal{D}$, since in components based on birefringent materials the extinctions for the fast and slow axes can be different (see e.g. [19]):

$$\mathcal{R} = \begin{bmatrix} 1 & 0 & 0 & 0 \\ 0 & 1 & 0 & 0 \\ 0 & 0 & C & -S \\ 0 & 0 & S & C \end{bmatrix} \tag{29}$$

$$\mathcal{D} = \frac{1}{2}\begin{bmatrix} P & \Delta & 0 & 0 \\ \Delta & P & 0 & 0 \\ 0 & 0 & X & 0 \\ 0 & 0 & 0 & X \end{bmatrix} \tag{30}$$

where $S = \sin(\phi), C = \cos(\phi), \phi$ is the phase delay introduced between the electric field components aligned to the fast and slow axes of the HWP, $P = p_x^2 + p_y^2$, $\Delta = p_x^2 - p_y^2$, $X = 2p_x p_y$, with $0 \leq p_x \leq 1$ and $0 \leq p_y \leq 1$ being the attenuation coefficients for the electric field components in the fast and slow axes respectively. An ideal HWP would have $P = 2, \Delta = 0, X = 2, \phi = \pi$. The Mueller matrix of the real HWP is

$$\mathcal{H} = \mathcal{R} \times \mathcal{D} = \frac{1}{2} \begin{bmatrix} P & \Delta & 0 & 0 \\ \Delta & P & 0 & 0 \\ 0 & 0 & CX & -SX \\ 0 & 0 & SX & CX \end{bmatrix} \tag{31}$$

When the HWP is rotated by an angle θ we have

$$\begin{aligned} \mathcal{H}(\theta) &= M_R(-2\theta) \times \mathcal{H} \times M_R(2\theta) = \\ &= \tfrac{1}{2} \begin{bmatrix} 1 & 0 & 0 & 0 \\ 0 & c_2 & -s_2 & 0 \\ 0 & s_2 & c_2 & 0 \\ 0 & 0 & 0 & 1 \end{bmatrix} \begin{bmatrix} P & \Delta & 0 & 0 \\ \Delta & P & 0 & 0 \\ 0 & 0 & CX & -SX \\ 0 & 0 & SX & CX \end{bmatrix} \begin{bmatrix} 1 & 0 & 0 & 0 \\ 0 & c_2 & s_2 & 0 \\ 0 & -s_2 & c_2 & 0 \\ 0 & 0 & 0 & 1 \end{bmatrix} = \\ &= \tfrac{1}{2} \begin{bmatrix} P & \Delta c_2 & \Delta s_2 & 0 \\ \Delta c_2 & P c_2^2 + CX s_2^2 & (P - CX) c_2 s_2 & s_2 XS \\ \Delta s_2 & (P - CX) s_2 c_2 & P s_2^2 + CX c_2^2 & -SX c_2 \\ 0 & -s_2 SX & c_2 SX & CX \end{bmatrix} \end{aligned} \tag{32}$$

where $s_2 = \sin(2\theta), c_2 = \cos(2\theta)$.

3.1.2 Polarimeter model

In a Stokes polarimeter, the input radiation with Stokes vector S crosses the HWP, which is followed by an ideal polarizer, whose main axis is either along x or along y, and finally is detected by an intensity detector with Stokes vector

$$D = [1 \quad 0 \quad 0 \quad 0] \tag{33}$$

Here we consider the measurement of polarization with is not circularly polarized, and is linearly polarized with polarization degree p and main axis angle α i.e.

$$S = I_o \begin{bmatrix} 1 \\ p\cos 2\alpha \\ p\sin 2\alpha \\ 0 \end{bmatrix} \tag{34}$$

So the power reaching the detector is

$$W_x = [1 \quad 0 \quad 0 \quad 0] \times P_x \times \mathcal{H}(\theta) \times I_o \begin{bmatrix} 1 \\ p\cos 2\alpha \\ p\sin 2\alpha \\ 0 \end{bmatrix} \tag{35}$$

where, assuming the main axis of the analyzer polarizer perfectly aligned to the x axis,

$$P_x = \mathcal{D}_{0,A} = \frac{1}{2}\begin{bmatrix} P_A & \Delta_A & 0 & 0 \\ \Delta_A & P_A & 0 & 0 \\ 0 & 0 & X_A & 0 \\ 0 & 0 & 0 & X_A \end{bmatrix} \tag{36}$$

Computing the products, we get:

$$\begin{aligned} W_x = \quad & \tfrac{I_o}{4}\Big[P_A P + \\ & + \Delta[pP_A\cos(2(\theta-\alpha)) + \Delta_A\cos(2\theta)] + \\ & + p\Delta_A[(P\cos^2(2\theta) + CX\sin^2(2\theta))\cos(2\alpha) + \\ & + (P - CX)\cos(2\theta)\sin(2\theta)\sin(2\alpha)]\Big] \end{aligned} \tag{37}$$

or equivalently

$$\begin{aligned} W_x = \quad & \tfrac{I_o}{4}\Big[P_A P + p\tfrac{\Delta_A}{2}(P + CX)\cos(2\alpha) + \\ & + \Delta[pP_A\cos(2\alpha) + \Delta_A]\cos(2\theta) + \Delta[pP_A\sin(2\alpha)]\sin(2\theta) + \\ & + p\tfrac{\Delta_A}{2}[(P - CX)\cos(4\theta - 2\alpha)]\Big] \end{aligned} \tag{38}$$

where the 4*f* signal due to the polarized fraction of the radiation under analysis is evident in the third line. We also note that, if the HWP transmission is not balanced ($\Delta \neq 0$), there is a spurious 2*f* modulation of the unpolarized intensity of the source (second line of (38)). Moreover, if the phase delay introduced by the HWP is not π (i.e. $-1 < C \leq 1$), the constant term is modified and the modulation efficiency of the polarized fraction is also reduced (first and last lines of (38)).

From (38) we see that the measurements of W_x for different orientations θ of the HWP can be described by the function

$$\begin{aligned} W_x = \quad & a + \\ & + b\cdot\cos(2\theta) + \\ & + c\cdot\sin(2\theta) + \\ & + d\cdot\cos(4\theta - 2\alpha) \end{aligned} \tag{39}$$

where

$$\begin{aligned} a &= \tfrac{I_o}{4}\left[P_A P + p\tfrac{\Delta_A}{2}(P + CX)\cos(2\alpha)\right] \\ b &= \tfrac{I_o}{4}\Delta[pP_A\cos(2\alpha) + \Delta_A] \\ c &= \tfrac{I_o}{4}\Delta pP_A\sin(2\alpha) \\ d &= \tfrac{I_o}{4}p\tfrac{\Delta_A}{2}(P - CX) \end{aligned} \tag{40}$$

are parameters which, together with α, can be retrieved from a best fit procedure. Since α is the only parameter appearing in a non-linear way in (39), an efficient way to perform the fit is to assume a value of α and perform a linear fit of (39) to retrieve the best fit values for parameters *a*, *b*, *c*, *d*. This process is very fast and can be repeated for a large set of values of α to find the values $\alpha^*, a^*, b^*, c^*, d^*$ producing the global minimum of the χ^2. This will produce our best estimate of the polarization direction of the source

$$\alpha = \alpha^*. \tag{41}$$

If the polarizer has been thoroughly characterized (i.e. Δ_A and P_A are known) and if deviations from ideality are small, using (40) one can obtain a zero-order estimate of the polarization degree of the source *p* from:

$$p_0 \simeq \frac{P_A}{\Delta_A} \cdot \frac{d^*}{a^*} \tag{42}$$

In order to obtain further insight on the approximation and on the effect of the non-ideality parameters, let's assume that the unbalance of the HWP is small and that the induced phase delay is close to π, i.e.

$$P = p_x^2 + p_y^2 = p_x^2 + p_x^2(1-\epsilon) = p_x^2(2-\epsilon) \tag{43}$$

$$\Delta = p_x^2 - p_y^2 = p_x^2\epsilon \tag{44}$$

$$X = 2p_x p_y \sim 2p_x^2(1-\epsilon) \tag{45}$$

$$C = \cos(\phi) = \cos(\pi + \delta\phi) \sim -1 + (\delta\phi)^2/2 \tag{46}$$

with $\epsilon \ll 1$ and $\delta\phi \ll 1$. Substituting in (40) we get a first order estimate of the polarization degree of the source:

$$p_1 \simeq \frac{P_A}{\Delta_A} \cdot \frac{d^*}{a^*}\left[1 + \left[\frac{\epsilon}{4} + \frac{(\delta\phi)^2}{4}\right] \cdot \left[1 + \frac{d^*}{a^*}\cos(2\alpha)\right]\right] \tag{47}$$

This means that an error $\delta\phi \sim 6^o$ in the phase delay introduced by the HWP results in less than 1% error in the zero order estimate of the polarization degree of the source p_0, while an unbalance $\epsilon \sim 5\%$ of the transmissions of the HWP results in less than 2% error in p_0.

The non ideality parameters of the HWP can be retrieved as follows.

Substituting the expressions of (43) and following into (40), we get two zero order estimates of the HWP trasmission unbalance ϵ , from the ratios b^*/a^* and c^*/a^*:

$$\begin{aligned} \epsilon_{0b} &\sim 2 \cdot \frac{b^*}{a^*} \cdot \frac{1}{p\cos(2\alpha) + \Delta_A/P_A} \\ \epsilon_{0c} &\sim 2 \cdot \frac{c^*}{a^*} \cdot \frac{1}{p\sin(2\alpha)} \end{aligned} \tag{48}$$

Depending on the value of α, one or the other equation can be used.

The phase delay error $\delta\phi$, instead, can be estimated comparing the values for the average signal a for totally polarized radiation ($p = 1$, a_1) and for totally unpolarized radiation ($p = 0$, a_0). Using the approximation of (43) we get

$$\epsilon + (\delta\phi)^2 \sim \frac{a_1 - a_0}{a_0} \frac{4P_A}{\Delta_A \cos(2\alpha)} \tag{49}$$

This is useful to estimate $\delta\phi$ when the nonideality due to the phase delay is dominant with respect to transmission unbalance.

Once the parameters describing the components are evaluated, the polarimeter response to a generic Stokes vector at the input can be derived in matrix form from (33)-(36). We get:

$$W_x = [1 \quad 0 \quad 0 \quad 0] \times R_x(\theta) \times \begin{bmatrix} I \\ Q \\ U \\ V \end{bmatrix} \tag{50}$$

where

$$R_x(\theta) = \\ = \frac{1}{2} \begin{bmatrix} [P_A P + \Delta_A \Delta c_2] & [P_A \Delta c_2 + \Delta_A (P c_2^2 + CX s_2^2)] & [P_A \Delta s_2 + \Delta_A (P - CX) c_2 s_2] & [\Delta_A s_2 XS] \\ [\Delta_A P + P_A \Delta c_2] & [\Delta_A \Delta c_2 + P_A (P c_2^2 + CX s_2^2)] & [\Delta_A \Delta s_2 + P_A (P - CX) c_2 s_2 & P_A s_2 XS] \\ [X_A \Delta s_2 & X_A (P - CX) s_2 c_2] & [X_A (P s_2^2 + CX c_2^2) & -X_A SX c_2] \\ [0] & [-s_2 SXX_A] & [c_2 SXX_A] & [CXX_A] \end{bmatrix} \tag{51}$$

is the *polarimeter response matrix* [14, 24]. When a set of n measurements of the source is taken for different orientations θ_j of the HWP, one obtains the *modulation matrix* of the measurement:

$$M_x = \\ = \frac{1}{2} \begin{bmatrix} [P_A P + \Delta_A \Delta c_2(\theta_1)] & [P_A \Delta c_2(\theta_1) + \Delta_A (P c_2^2(\theta_1) + CX s_2^2(\theta_1))] & [P_A \Delta s_2(\theta_1) + \Delta_A (P - CX) c_2(\theta_1) s_2(\theta_1] & [\Delta_A s_2(\theta_1) XS] \\ \dots & \dots & \dots & \dots \\ \dots & \dots & \dots & \dots \\ [P_A P + \Delta_A \Delta c_2(\theta_n)] & [P_A \Delta c_2(\theta_n) + \Delta_A (P c_2^2(\theta_n) + CX s_2^2(\theta_n))] & [P_A \Delta s_2(\theta_n) + \Delta_A (P - CX) c_2(\theta_n) s_2(\theta_n)] & [\Delta_A s_2(\theta_n) XS] \end{bmatrix} \tag{52}$$

such that the vector of the measurements can be written

$$W_x = M_x \times \begin{bmatrix} I \\ Q \\ U \\ V \end{bmatrix} \tag{53}$$

This equation can be inverted to retrieve the Stokes vector of the source from the measurements and to propagate the measurement uncertainties (see [24] for a discussion). Using the calibration procedure described here, we can constrain the parameters P_A, P, Δ_A, Δ, C, S, X, (or, in case of small deviations from ideality, the parameters listed

in (43) and following) so that the polarimeter response matrix and the modulation matrix of the measurement can be estimated (see Section 3.2.3).

3.2 Measurements

3.2.1 High polarization degree

We setup the Stokes polarimeter on the optical bench used for the polarizer measurements, by adding the HWP on a rotating support between the purifying polarizer and the analyzer polarizer (see Fig. 4).

In this case we can consider the radiation illuminating the HWP as fully linearly polarized. The signal detected as a function of the rotation angle of the HWP θ is shown in Fig. 5. The HWP has been rotated in steps of 11.25^o, integrating for 3s in each position. To obtain 5 full rotations of the HWP a total measurement time of ~ 10 minutes is required.

As expected, the signal is modulated at 4*f*. The total cancellation of the signal at the minima confirms the very high polarization degree of the laser diode source followed by a purifying polarizer. The lack of a 2*f* signal confirms a good balance of the HWP: from the best fit (39), using (42) we estimate

$$p_0 = 0.9982 \pm 0.0002 \tag{54}$$

(1-σ statistical error only) and (43):

$$\Delta/p_x^2 = \epsilon \sim 3 \times 10^{-4} \tag{55}$$

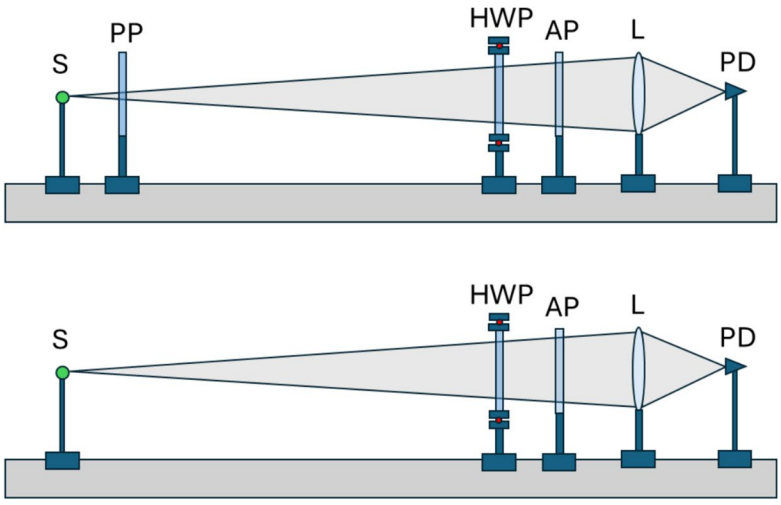

Fig. 4 **Top:** Measurement setup for the characterization of the HWP and polarimeter. From left to right: laser diode source (S), purifying polarizer (PP), Half Wave Plate with its rotary stage (HWP), analyzer polarizer (AP), lens (L), photodetector (PD). **Bottom:** Measurement setup for the characterization of the polarimeter in case the polarization degree of the source is not close to unity. In this case S can be either a green laser diode or a green LED

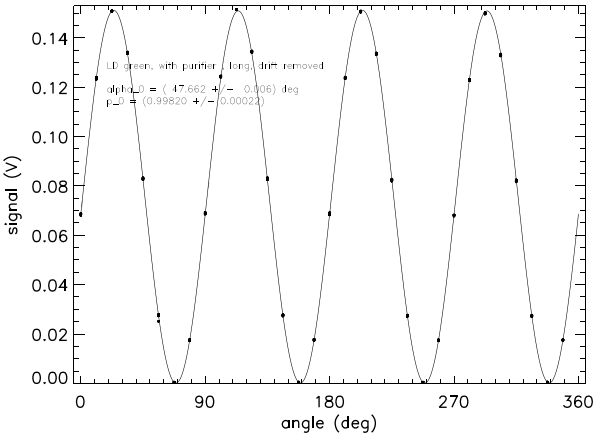

Fig. 5 Measured signal vs rotation angle θ of the HWP, for a totally polarized source. The measured data for 5 full rotations of the HWP are plotted as squares. The continuous line is the best fit of the data using (39)

confirming a very good balance for the transmissions of the fast and slow axes of the HWP.

In order to test the performance of the polarimeter when the polarization degree of the source is not very close to 1, we first remove the purifying polarizer. As we have seen, this leaves us with a source (the green laser diode) which is not totally polarized. The signal detected as a function of the rotation angle of the HWP θ is shown in Fig. 6.

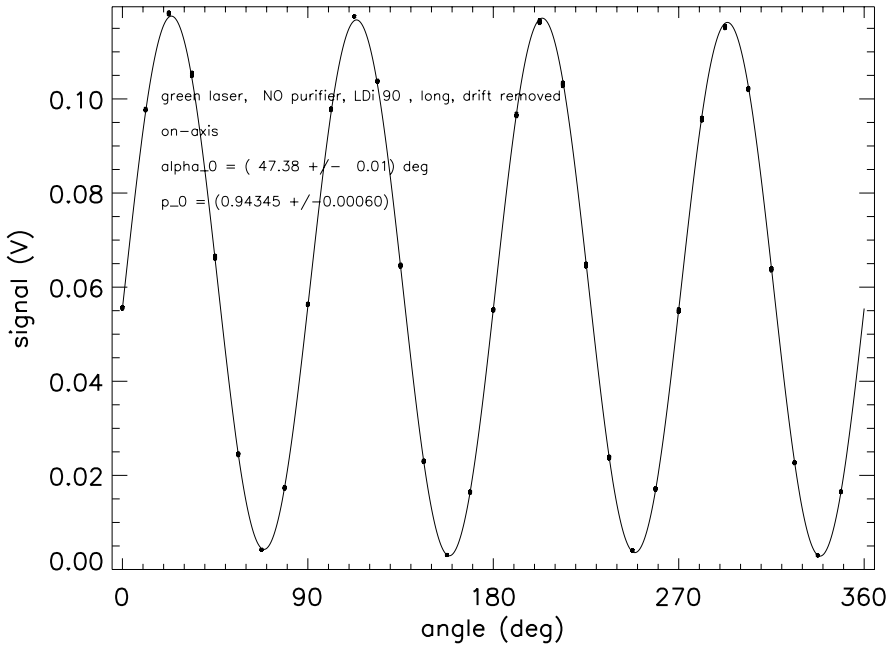

Fig. 6 Measured signal vs rotation angle θ of the HWP, for a partially polarized source. The measured data for 5 full rotations of the HWP are plotted as squares. The partial polarization of the source is evident, since the minima of the signal do not reach zero. The continuous line is the best fit of the data using (38)

As we can see, the polarimeter clearly detects partial polarization, since the minima are not reaching zero. Fitting the data with (38) we find a polarization degree of 94% for the laser diode source, which is basically consistent with the specs from the manufacturer.

3.2.2 Low polarization degree

In order to test the performance of the polarimeter when the polarization degree of the source is $\ll 1$ (which is the relevant case for starlight polarization surveys), we remove the purifying polarizer, and substitute the green laser diode with a green LED diode. This has a low degree of linear polarization, depending on the alignment of the LED plastic enclosure with respect to the optical axis (see e.g. [25]). The detected signal vs the rotation angle of the HWP is reported in the top panel of Fig. 7.

In addition to the 4*f* modulation of the signal, which points to a small polarization degree of the source (as low as $p \sim 0.003$), we confirm the lack of significant 2*f* components, while a 1*f* component producing a signal with amplitude similar to the one of the 4*f* component is due to small misalignments in the system. In order to demonstrate that the 4*f* component of the signal is intrinsic to the source, we rotate it around the optical axis and repeat the measurement. The result is plotted in the bottom panel of Fig. 7. As expected, the phase of the 4*f* component shifts with respect to the case shown in the left panel. The shift in the other parameters is small and is likely due to the increase of the polarization degree of the LED when it is not seen perfectly on-axis [25].

In order to establish the repeatibility of this setup for the measurement of small polarization degrees, we repeat 20 times the measurement of 5 full rotations of the HWP (~ 10 minutes), switching off completely the apparatus, realigning the optical elements, and waiting a warm-up time of 10 minutes prior to each repetition. The average polarization degree is found to be $\langle p \rangle = 0.9910\%$ with a standard deviation $\sigma_p = 0.0013\%$; for the position angle we find $\langle \alpha \rangle = 62.352^o$ with a standard deviation $\sigma_\alpha = 0.045^o$. We conclude that the setup is reproducible at the $\sim 10^{-5}$ level for polarization degree measurements, and at a level of $\sim 3'$ for position angle measurements.

3.2.3 Polarimeter matrix

In order to estimate the polarimeter matrix we also need a measurement of the HWP transmission. We use the bottom configuration of Fig. 4, with unpolarized radiation and removing the analyzing polarizer. The ratio of the signal detected with and without HWP is $p_x^2 = (0.917 \pm 0.003)$. At this point we can use the results obtained so far for the components parameters (P_A, Δ_A, p_x^2, ϵ, $(\delta\phi)^2$) and (43) to (51) to write explicitly the polarimeter matrix. We find

$$R_{x,meas} = \\ = \begin{bmatrix} [0.7931{+}0.00012c_2] & [0.00012c_2{+}0.7931c_2^2{-}0.7930s_2^2] & [0.00012s_2{+}1.586c_2s_2] & [-0.0040s_2] \\ [0.7931{+}0.00012c_2] & [0.00012c_2{+}0.7931c_2^2{-}0.7930s_2^2] & [0.00012s_2{+}1.586c_2s_2] & [-0.0040s_2] \\ [1.4{\times}10^{-8}s_2] & [0.00018s_2c_2] & [9.2{\times}10^{-5}s_2^2{-}9.2{\times}10^{-5}c_2^2] & [4.6{\times}10^{-7}c_2] \\ 0 & [0.00018s_2] & [4.6{\times}10^{-7}c_2] & -9.2{\times}10^{-5} \end{bmatrix} \quad (56)$$

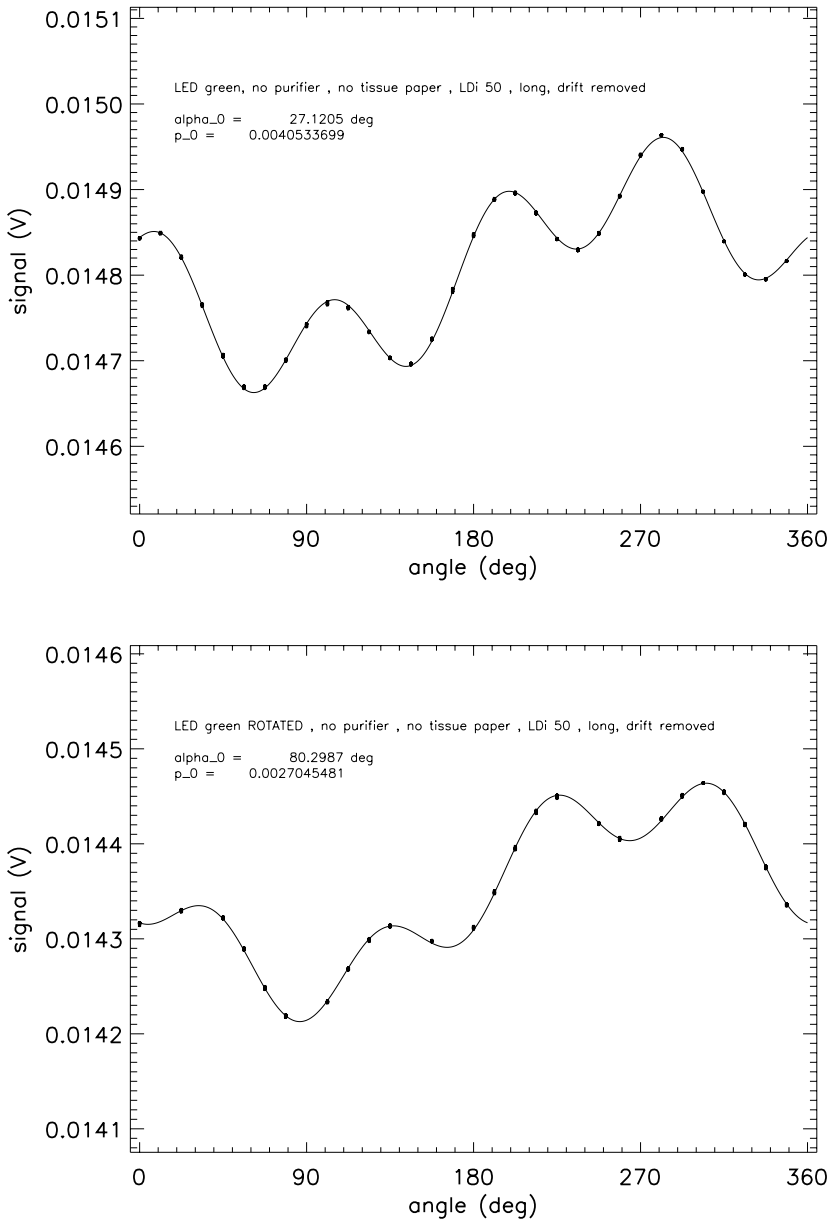

Fig. 7 **Top:** Measured signal vs rotation angle θ of the HWP, for a green LED source with a small polarization degree. The measured data for 5 full rotations of the HWP are plotted as squares. The continuous line is the best fit of the data using (38) with additional $1f$ terms. **Bottom:** Same as the top figure, after a rotation of the LED source along the optical axis

Here the numbers in *italics* represent upper limits (deriving from our upper limits on Δ, X_A and $(\delta\phi)^2$), while the measurement error for the other numbers is of the order of the least significant digit. Apart from a global efficiency ($\sim 79\%$), such a matrix features only small deviations from the one of the Stokes polarimeter assembled with ideal components

$$R_{x,ideal} = \begin{bmatrix} [1] & [c_2^2 - s_2^2] & [2c_2 s_2] & [0] \\ [1] & [c_2^2 - s_2^2] & [2c_2 s_2] & [0] \\ [0] & [0] & [0] & [0] \\ [0] & [0] & [0] & [0] \end{bmatrix} \tag{57}$$

The estimate of R_x allows to evaluate the modulation matrix (52) as a function of the observation strategy (i.e. the set of observed orientations θ_j) and to optimize the measurement campaign by properly taking into account the propagation of measurement errors [14, 24]. To this purpose several additional factors, like the selected targets, the observation site, the total survey duration, its efficiency, and the performance of the detector system must be defined.

4 Response to slant incidence rays

In an imaging Stokes polarimeter, off-axis pixels receive radiation that crosses the HWP and the polarizer at a slant angle. Under these conditions, projection effects and the increased optical path through the HWP—introducing a retardance that deviates from exactly π—slightly reduce the modulation efficiency of the polarimeter. This results in a systematic underestimation of the source's polarization degree. To assess these effects, we tested the performance of the HWP for tilted incidence angles i, up to $\pm 6^o$ with respect to normal incidence, while keeping the same source. To better investigate the effects of tilted incidence, we used the polarized laser source without any purifying polarizer, and the instrument configuration shown in Fig. 8.

We analyzed the data without accounting for slant incidence in the theoretical model, i.e. using (39), which is strictly valid only for on-axis incidence. The results are summarized in Table 2 and in Fig. 9. The error bars are dominated by the uncertainty in the incidence angle i in our experimental setup.

We find that applying this simplified analysis procedure (i.e. using the normal-incidence formulas even for incidence angles up to 6^o off-axis) introduces small but detectable systematic effects in the retrieved polarization properties of the source. We refer to these effects as the *off-axis bias*.

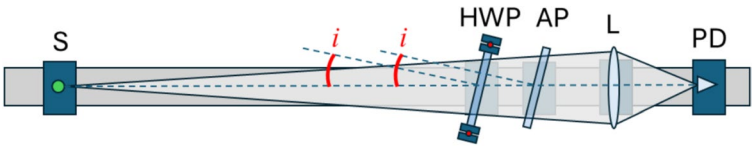

Fig. 8 Setup to measure the response of the polarimeter to slant incidence angles i

Table 2 Retrieved polarization properties of a given source when its light undergoes slant incidence on the HWP and polarizer, and a simplistic analysis procedure is used

i (^{o})	-6	-3	0	$+3$	$+6$
p (%)	93.77 ± 0.05	94.18 ± 0.02	94.34 ± 0.02	94.21 ± 0.02	93.52 ± 0.12
α (^{o})	47.58 ± 0.03	47.43 ± 0.02	47.37 ± 0.02	47.42 ± 0.03	47.64 ± 0.04

The p and α values are retrieved from a best fit using (39), i.e. neglecting slant incidence

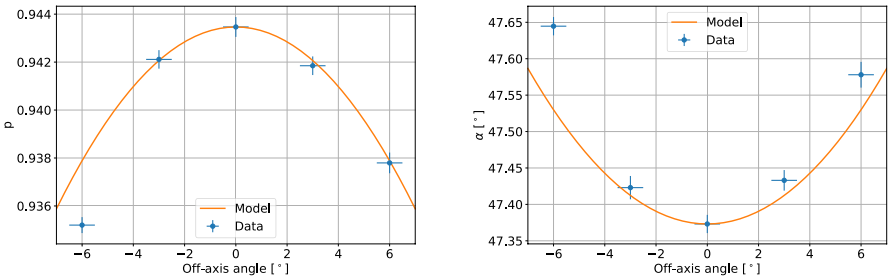

Fig. 9 **Left:** Retrieved polarization degree of the source versus incidence angle for off-axis incidence up to $\pm 6^\circ$. **Right:** The same for the polarization direction of the source. The error bars are statistical only. The lines represent the prediction from the theory described in Appendix A

Following the approach described in [23] (see Appendix A), we simulated the expected modulated signal as a function of the HWP rotation angle for different positions in the focal plane, and fitted the simulated signal to retrieve the expected biased estimates of the source polarization properties. These can be compared to the values reported in Table 2. The measured *off-axis bias* is consistent with these predictions, and is small: the largest bias for the polarization degree is of the order of 1% at 6° off-axis, while the largest bias for the polarization direction is of the order of 0.25° at 6° off-axis.

Using the approach described in Appendix A we have computed the *off-axis bias* for several off-axis directions uniformly distributed across a $10^o \times 5^o$ field of view (FOV) and for the source configuration considered in Table 2. The results are shown in Fig. 10 and can be used to correct for off-axis biases.

Alternatively, the analytical formulas described in Appendix A, can be used to fit the measured data. Although it comes at the cost of added complexity, this allows the polarization properties of the source to be retrieved without introducing bias. Since the deviations are very small, error propagation is essentially the same as for the on-axis pixel analyzed in detail in the previous sections.

5 Discussion and conclusions

The measurement setup and sequence of measurements described in this paper have proven to be reproducible at the level of $\sim 10^{-5}$ for polarization degree measurements, and at the level of $\sim 3'$ for position angle measurements. This setup makes it possible to assess the performance of a polarizer and an HWP in the visual band,

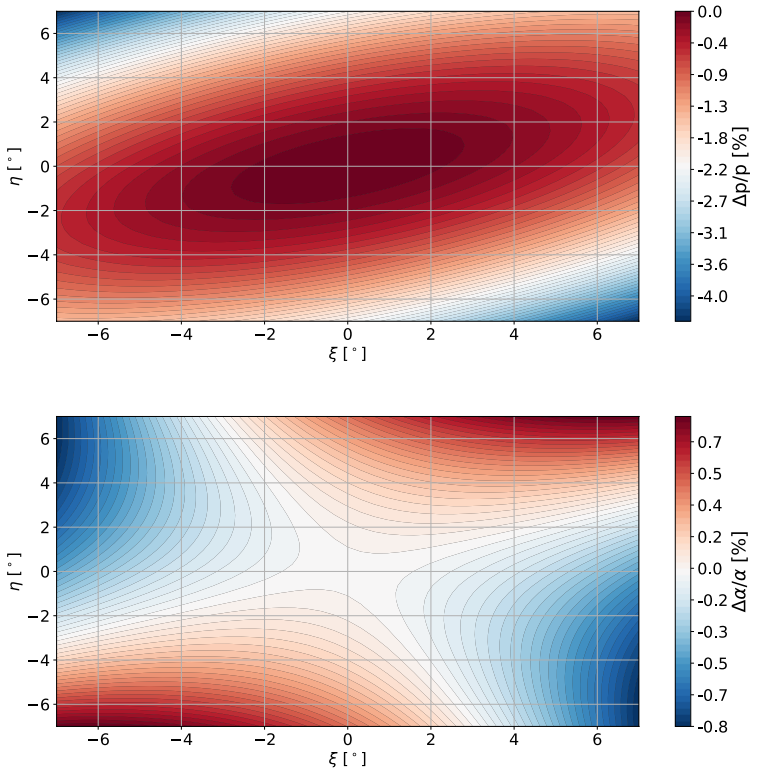

Fig. 10 **Top:** Expected fractional difference between the reconstructed and the input polarization degree of the source, computed as a function of the off-axis angles ξ and η, for a $10^o \times 5^o$ focal plane (see Appendix A) . **Bottom:** The same for the polarization direction

with a sensitivity of $\sim 10^{-4}$ for both the cross-polarization of the polarizer and the transmission imbalance of the HWP.

We find that the tested components are suitable for measuring polarization degrees down to $p \simeq 10^{-4}$. This roughly defines the sensitivity target for a stellar polarization survey using these components. In fact, when applied to starlight polarization measurements, their optical aperture ($\sim$ 10 cm in diameter) allows measurements of the polarization degree with a sensitivity of $\sim 10^{-3}$ in 30 seconds of integration for stars of $m_V \sim 9$. If the sky background permits, even longer integrations are possible before systematic effects become limiting.

The excellent performance at tilted angles (up to 6^o off-axis with only a small and correctable bias in the polarimetry), as described in §4, permits the implementation of an imaging polarimeter based on these components with a $10^o \times 5^o$ FOV. Under these conditions, polarimetric measurements of tens of stars with $m_V < 9$ can be achieved in 30 seconds of integration.

We are currently building a small Stokes polarimeter based on these components to experimentally test the end-to-end performance, with a view toward a future ultra-low-background space-based implementation of this instrument concept.

Appendix A: Response of a Stokes polarimeter for slant incidence

Here, we compute the response of a Stokes polarimeter to slant-incidence rays, following the approach described in [23], but extending the analysis to the case of slant incidence on both the HWP and the polarizer. To keep the formulas from becoming unmanageably complex, we assume that both components are ideal, since the actual components of interest here are indeed very close to ideal. The input Stokes vector in the 3D formalism (see e.g. [26]) can be defined as:

$$\mathbf{s_{in}} = \begin{bmatrix}\Delta_0\\ \Delta_1\\ \Delta_2\\ \Delta_3\\ \Delta_4\\ \Delta_5\\ \Delta_6\\ \Delta_7\\ \Delta_8\end{bmatrix} = \begin{bmatrix} \frac{1}{\sqrt{3}}\left(\langle E_xE_x^*\rangle + \langle E_yE_y^*\rangle + \langle E_zE_z^*\rangle\right)\\ \frac{1}{\sqrt{2}}\left(\langle E_xE_y^*\rangle + \langle E_yE_x^*\rangle\right)\\ \frac{1}{\sqrt{2}}\left(\langle E_zE_x^*\rangle + \langle E_xE_z^*\rangle\right)\\ \frac{i}{\sqrt{2}}\left(\langle E_xE_y^*\rangle - \langle E_yE_x^*\rangle\right)\\ \frac{1}{\sqrt{2}}\left(\langle E_xE_x^*\rangle - \langle E_yE_y^*\rangle\right)\\ \frac{1}{\sqrt{2}}\left(\langle E_yE_z^*\rangle + \langle E_zE_y^*\rangle\right)\\ \frac{i}{\sqrt{2}}\left(\langle E_zE_x^*\rangle - \langle E_xE_z^*\rangle\right)\\ \frac{i}{\sqrt{2}}\left(\langle E_yE_z^*\rangle - \langle E_zE_y^*\rangle\right)\\ \frac{1}{\sqrt{6}}\left(\langle E_xE_x^*\rangle + \langle E_yE_y^*\rangle - 2\langle E_zE_z^*\rangle\right)\end{bmatrix} = \begin{bmatrix} \frac{1}{\sqrt{3}}\left(\langle E_xE_x^*\rangle + \langle E_yE_y^*\rangle\right)\\ \frac{1}{\sqrt{2}}\left(\langle E_xE_y^*\rangle + \langle E_yE_x^*\rangle\right)\\ 0\\ \frac{i}{\sqrt{2}}\left(\langle E_xE_y^*\rangle - \langle E_yE_x^*\rangle\right)\\ \frac{1}{\sqrt{2}}\left(\langle E_xE_x^*\rangle - \langle E_yE_y^*\rangle\right)\\ 0\\ 0\\ 0\\ \frac{1}{\sqrt{6}}\left(\langle E_xE_x^*\rangle + \langle E_yE_y^*\rangle\right)\end{bmatrix} \quad \text{(A1)}$$

where the rightmost equality is due to the fact that the *z* axis is aligned with the light propagation direction in our reference system. The output Stokes vector is:

$$\mathbf{s_{out}} = M_{pol}(\eta,\xi)\cdot M_{HWP}(\eta,\xi,\theta)\cdot \mathbf{s_{in}} \quad \text{(A2)}$$

where ξ and η are the two angles (azimuth and elevation) defining the off-axis direction, θ is the rotation angle of the HWP (around its symmetry axis), $M_{pol}(\eta,\xi)$ and $M_{HWP}(\eta,\xi,\theta)$ are the matrices describing the response of the *tilted* ideal polarizer and HWP. Both matrices for the normal incidence case are obtained from the associated Jones ones (*J*) using the Gell-Mann [27] matrices σ_n :

$$M_{ij} = tr(\sigma_i\cdot J\cdot\sigma_j\cdot J^{\top}). \quad \text{(A3)}$$

We obtain

$$M_{HWP}(\theta) = \begin{bmatrix} 1 & 0 & 0 & 0 & 0 & 0 & 0 & 0 & 0 \\ 0 & -\cos(4\theta) & 0 & 0 & \sin(4\theta) & 0 & 0 & 0 & 0 \\ 0 & 0 & \cos(2\theta) & 0 & 0 & \sin(2\theta) & 0 & 0 & 0 \\ 0 & 0 & 0 & -1 & 0 & 0 & 0 & 0 & 0 \\ 0 & \sin(4\theta) & 0 & 0 & \cos(4\theta) & 0 & 0 & 0 & 0 \\ 0 & 0 & \sin(2\theta) & 0 & 0 & -\cos(2\theta) & 0 & 0 & 0 \\ 0 & 0 & 0 & 0 & 0 & 0 & \cos(2\theta) & -\sin(2\theta) & 0 \\ 0 & 0 & 0 & 0 & 0 & 0 & -\sin(2\theta) & -\cos(2\theta) & 0 \\ 0 & 0 & 0 & 0 & 0 & 0 & 0 & 0 & 1 \end{bmatrix} \tag{A4}$$

$$M_{pol} = \begin{bmatrix} \frac{1}{3} & 0 & 0 & 0 & \frac{\sqrt{6}}{6} & 0 & 0 & 0 & \frac{\sqrt{2}}{6} \\ 0 & 0 & 0 & 0 & 0 & 0 & 0 & 0 & 0 \\ 0 & 0 & 0 & 0 & 0 & 0 & 0 & 0 & 0 \\ 0 & 0 & 0 & 0 & 0 & 0 & 0 & 0 & 0 \\ \frac{\sqrt{6}}{6} & 0 & 0 & 0 & \frac{1}{2} & 0 & 0 & 0 & \frac{\sqrt{3}}{6} \\ 0 & 0 & 0 & 0 & 0 & 0 & 0 & 0 & 0 \\ 0 & 0 & 0 & 0 & 0 & 0 & 0 & 0 & 0 \\ 0 & 0 & 0 & 0 & 0 & 0 & 0 & 0 & 0 \\ \frac{\sqrt{2}}{6} & 0 & 0 & 0 & \frac{\sqrt{3}}{6} & 0 & 0 & 0 & \frac{1}{6} \end{bmatrix}. \tag{A5}$$

Rotation matrices are used to compute the matrices for the tilted incidence case:

$$M_{pol}(\eta, \xi) = R(\eta, \xi) \cdot M_{pol} \cdot R(-\eta, -\xi) \tag{A6}$$

$$M_{HWP}(\eta, \xi, \theta) = R(\eta, \xi) \cdot M_{HWP}(\theta) \cdot R(-\eta, -\xi) \tag{A7}$$

where the rotation matrix

$$R(\eta, \xi) = M_{RotX}(\eta) \cdot M_{RotY}(\xi) \tag{A8}$$

is the product of the two rotation matrices

$$M_{RotX}(\eta) = \begin{bmatrix} 1 & 0 & 0 & 0 & 0 & 0 & 0 & 0 & 0 \\ 0 & \cos(\eta) & 0 & 0 & 0 & \sin(\eta) & 0 & 0 & 0 \\ 0 & 0 & \cos(2\eta) & 0 & -\frac{1}{2}\sin(2\eta) & 0 & 0 & 0 & -\frac{\sqrt{3}}{2}\sin(2\eta) \\ 0 & 0 & 0 & \cos(\eta) & 0 & 0 & 0 & \sin(\eta) & 0 \\ 0 & 0 & \frac{1}{2}\sin(2\eta) & 0 & \frac{1}{2}\cos^2(\eta) + \frac{1}{2} & 0 & 0 & 0 & -\frac{\sqrt{3}}{2}\sin^2(\eta) \\ 0 & -\sin(\eta) & 0 & 0 & 0 & \cos(\eta) & 0 & 0 & 0 \\ 0 & 0 & 0 & 0 & 0 & 0 & 1 & 0 & 0 \\ 0 & 0 & 0 & -\sin(\eta) & 0 & 0 & 0 & \cos(\eta) & 0 \\ 0 & 0 & \frac{\sqrt{3}}{2}\sin(2\eta) & 0 & -\frac{\sqrt{3}}{2}\sin^2(\eta) & 0 & 0 & 0 & -\frac{3}{2}\sin^2(\eta) + 1 \end{bmatrix} \tag{A9}$$

$$M_{RotY}(\xi) = \begin{bmatrix} 1 & 0 & 0 & 0 & 0 & 0 & 0 & 0 & 0 \\ 0 & \cos(\xi) & -\sin(\xi) & 0 & 0 & 0 & 0 & 0 & 0 \\ 0 & \sin(\xi) & \cos(\xi) & 0 & 0 & 0 & 0 & 0 & 0 \\ 0 & 0 & 0 & \cos(\xi) & 0 & 0 & -\sin(\xi) & 0 & 0 \\ 0 & 0 & 0 & 0 & \frac{1}{2}\cos^2(\xi)+\frac{1}{2} & \frac{1}{2}\sin(2\xi) & 0 & 0 & \frac{\sqrt{3}}{2}\sin^2(\xi) \\ 0 & 0 & 0 & 0 & -\frac{1}{2}\sin(2\xi) & \cos(2\xi) & 0 & 0 & \frac{\sqrt{3}}{2}\sin(2\xi) \\ 0 & 0 & 0 & \sin(\xi) & 0 & 0 & \cos(\xi) & 0 & 0 \\ 0 & 0 & 0 & 0 & 0 & 0 & 0 & 1 & 0 \\ 0 & 0 & 0 & 0 & \frac{\sqrt{3}}{2}\sin^2(\xi) & -\frac{\sqrt{3}}{2}\sin(2\xi) & 0 & 0 & -\frac{3}{2}\sin^2(\xi)+1 \end{bmatrix} \tag{A10}$$

Comparing to the definition of the regular 2D Stokes parameters, we find that the conventional 2D Stokes parameters are related to the 3D Stokes parameters (optical ordering) by the following relations:

$$I = \sqrt{\frac{2}{3}}\left(\Delta_0 + \frac{\Delta_8}{\sqrt{2}}\right), \qquad Q = \Delta_4, \qquad U = \Delta_1, \qquad V = \Delta_3. \tag{A11}$$

The total intensity measured is then:

$$W = \cos^2(\xi)(a_0\Delta_0 + a_1\Delta_1 + a_4\Delta_4 + a_8\Delta_8) \tag{A12}$$

where

$$a_0 = \frac{1}{2}\sqrt{\frac{2}{3}} \tag{A13}$$

$$a_1 = \cos(\eta)\left[\sin(\xi)\sin(\eta)\big(1-\cos^2(2\theta)\big) + \sin(2\theta)\cos(\xi)\cos(2\theta)\right] \tag{A14}$$

$$\begin{aligned} a_4 = \Big[& \sin(\xi)\sin(\eta)\sin(2\theta)\cos(\xi)\cos(2\theta) + \cos^2(\xi)\big(\cos^2(2\theta) - \frac{1}{2}\big) \\ & + \frac{1}{2}\big(\cos^2(\xi)\cos^2(\eta) - 2\cos^2(\eta) + 1\big)\big(1-\cos^2(2\theta)\big)\Big] \end{aligned} \tag{A15}$$

$$\begin{aligned} a_8 = \sqrt{3}\Big[& \sin(\xi)\sin(\eta)\sin(2\theta)\cos(\xi)\cos(2\theta) + \frac{1}{2}\cos^2(\xi)\cos^2(\eta)\big(1-\cos^2(2\theta)\big) \\ & + \cos^2(\xi)\big(\cos^2(2\theta) - \frac{1}{2}\big) + \frac{1}{2}\big(\frac{1}{3} - \cos^2(2\theta)\big)\Big] \end{aligned} \tag{A16}$$

Equation (A12) is used to compute the simulated the data presented in Figs. 9 and 10.

Acknowledgements The optical components used in this paper have been funded by *Next generation EU*, Italian PNRR (Piano Nazionale di Ripresa e Resilienza), within the INAF project EMM (Earth Moon Mars).

Author Contributions PdB and SM designed the instrument and carried out the measurements. All authors developed the theoretical framework, carried out the data analysis, wrote the main manuscript text and reviewed the manuscript.

Data Availability Data sets generated during the current study are available from the corresponding author on reasonable request.

Declarations

Competing interests The authors declare no competing interests.

References

1. Hiltner, W.A.: Polarization of stellar radiation. III. The polarization of 841 stars. Astrophys. J. **114**, 241 (1951). https://doi.org/10.1086/145465
2. Davis, L., Greenstein, J.L.: The polarization of starlight by aligned dust grains. Astrophys. J. **114**, 206 (1951). https://doi.org/10.1086/145464
3. Spitzer, L., Tukey, J.W.: A theory of interstellar polarization. Astrophys. J. **114**, 187 (1951). https://doi.org/10.1086/145463
4. Draine, B.T.: Interstellar dust grains. Annu. Rev. Astron. Astrophys. **41**, 241–289 (2003). https://doi.org/10.1146/annurev.astro.41.011802.094840, arXiv:2106.08031 [astro-ph.CO]
5. Skalidis, R., Panopoulou, G.V., Tassis, K., Pavlidou, V., Blinov, D., Komis, I., Liodakis, I.: Local measurements of the mean interstellar polarization at high Galactic latitudes. Astron. Astrophys. **616**, 52 (2018). https://doi.org/10.1051/0004-6361/201832827. arXiv:astro-ph/0304489 [astro-ph]

6. Planck Collaboration, Ade, P.A.R., Aghanim, N., Alina, D., Alves, M.I.R., Armitage-Caplan, C., Arnaud, M., Arzoumanian, D., Ashdown, M., Atrio-Barandela, F., Aumont, J., Baccigalupi, C., Banday, A.J., Barreiro, R.B., Battaner, E., Benabed, K., Benoit-Lévy, A., Bernard, J.-P., Bersanelli, M., Bielewicz, P., Bock, J.J., Bond, J.R., Borrill, J., Bouchet, F.R., Boulanger, F., Bracco, A., Burigana, C., Butler, R.C., Cardoso, J.-F., Catalano, A., Chamballu, A., Chary, R.-R., Chiang, H.C., Christensen, P.R., Colombi, S., Colombo, L.P.L., Combet, C., Couchot, F., Coulais, A., Crill, B.P., Curto, A., Cuttaia, F., Danese, L., Davies, R.D., Davis, R.J., de Bernardis, P., de Gouveia Dal Pino, E.M., de Rosa, A., de Zotti, G., Delabrouille, J., Désert, F.-X., Dickinson, C., Diego, J.M., Donzelli, S., Doré, O., Douspis, M., Dunkley, J., Dupac, X., Efstathiou, G., Enßlin, T.A., Eriksen, H.K., Falgarone, E., Ferrière, K., Finelli, F., Forni, O., Frailis, M., Fraisse, A.A., Franceschi, E., Galeotta, S., Ganga, K., Ghosh, T., Giard, M., Giraud-Héraud, Y., González-Nuevo, J., Górski, K.M., Gregorio, A., Gruppuso, A., Guillet, V., Hansen, F.K., Harrison, D.L., Helou, G., Hernández-Monteagudo, C., Hildebrandt, S.R., Hivon, E., Hobson, M., Holmes, W.A., Hornstrup, A., Huffenberger, K.M., Jaffe, A.H., Jaffe, T.R., Jones, W.C., Juvela, M., Keihänen, E., Keskitalo, R., Kisner, T.S., Kneissl, R., Knoche, J., Kunz, M., Kurki-Suonio, H., Lagache, G., Lähteenmäki, A., Lamarre, J.-M., Lasenby, A., Lawrence, C.R., Leahy, J.P., Leonardi, R., Levrier, F., Liguori, M., Lilje, P.B., Linden-Vørnle, M., López-Caniego, M., Lubin, P.M., Macías-Pérez, J.F., Maffei, B., Magalhães, A.M., Maino, D., Mandolesi, N., Maris, M., Marshall, D.J., Martin, P.G., Martínez-González, E., Masi, S., Matarrese, S., Mazzotta, P., Melchiorri, A., Mendes, L., Mennella, A., Migliaccio, M., Miville-Deschênes, M.-A., Moneti, A., Montier, L., Morgante, G., Mortlock, D., Munshi, D., Murphy, J.A., Naselsky, P., Nati, F., Natoli, P., Netterfield, C.B., Noviello, F., Novikov, D., Novikov, I., Oxborrow, C.A., Pagano, L., Pajot, F., Paladini, R., Paoletti, D., Pasian, F., Pearson, T.J., Perdereau, O., Perotto, L., Perrotta, F., Piacentini, F., Piat, M., Pietrobon, D., Plaszczynski, S., Poidevin, F., Pointecouteau, E., Polenta, G., Popa, L., Pratt, G.W., Prunet, S., Puget, J.-L., Rachen, J.P., Reach, W.T., Rebolo, R., Reinecke, M., Remazeilles, M., Renault, C., Ricciardi, S., Riller, T., Ristorcelli, I., Rocha, G., Rosset, C., Roudier, G., Rubiño-Martín, J.A., Rusholme, B., Sandri, M., Savini, G., Scott, D., Spencer, L.D., Stolyarov, V., Stompor, R., Sudiwala, R., Sutton, D., Suur-Uski, A.-S., Sygnet, J.-F., Tauber, J.A., Terenzi, L., Toffolatti, L., Tomasi, M., Tristram, M., Tucci, M., Umana, G., Valenziano, L., Valiviita, J., Van Tent, B., Vielva, P., Villa, F., Wade, L.A.: Planck intermediate results. XIX. An overview of the polarized thermal emission from Galactic dust. Astron. Astrophys. **576**, 104 (2015). https://doi.org/10.1051/0004-6361/201424082. arXiv:1405.0871 [astro-ph.GA]
7. Stokes, G.G.: On the composition and resolution of streams of polarized light from different sources. Trans. Cambridge Philos. Soc. **9**, 399 (1851)
8. Skinner, C.A.: A universal polarimeter*. J. Opt. Soc. Am. (1917-1983) **10**(4), 491 (1925). https://doi.org/10.1364/JOSA.10.000491
9. Kusaka, A., Appel, J., Essinger-Hileman, T., Beall, J.A., Campusano, L.E., Cho, H.-M., Choi, S.K., Crowley, K., Fowler, J.W., Gallardo, P., Hasselfield, M., Hilton, G., Ho, S.-P.P., Irwin, K., Jarosik, N., Niemack, M.D., Nixon, G.W., Nolta, M., Page, L.A. Jr., Palma, G.A., Parker, L., Raghunathan, S., Reintsema, C.D., Sievers, J., Simon, S.M., Staggs, S.T., Visnjic, K., Yoon, K.-W.: Results from the Atacama B-mode Search (ABS) experiment. J. Cosmol. Astropart. Phys. **2018**(9), 005 (2018). https://doi.org/10.1088/1475-7516/2018/09/005. arXiv:1405.0871 [astro-ph.GA]
10. Takakura, S., Aguilar, M., Akiba, Y., Arnold, K., Baccigalupi, C., Barron, D., Beckman, S., Boettger, D., Borrill, J., Chapman, S., Chinone, Y., Cukierman, A., Ducout, A., Elleflot, T., Errard, J., Fabbian, G., Fujino, T., Galitzki, N., Goeckner-Wald, N., Halverson, N.W., Hasegawa, M., Hattori, K., Hazumi, M., Hill, C., Howe, L., Inoue, Y., Jaffe, A.H., Jeong, O., Kaneko, D., Katayama, N., Keating, B., Keskitalo, R., Kisner, T., Krachmalnicoff, N., Kusaka, A., Lee, A.T., Leon, D., Lowry, L., Matsuda, F., Matsumura, T., Navaroli, M., Nishino, H., Paar, H., Peloton, J., Poletti, D., Puglisi, G., Reichardt, C.L., Ross, C., Siritanasak, P., Suzuki, A., Tajima, O., Takatori, S., Teply, G.: Performance of a continuously rotating half-wave plate on the polarbear telescope. J. Cosmol. Astropart. Phys. **2017**(5), 008 (2017). https://doi.org/10.1088/1475-7516/2017/05/008
11. Bagnulo, S., Cox, N.L.J., Cikota, A., Siebenmorgen, R., Voshchinnikov, N.V., Patat, F., Smith, K.T., Smoker, J.V., Taubenberger, S., Kaper, L., Cami, J., LIPS Collaboration: Large Interstellar Polarisation Survey (LIPS). I. FORS2 spectropolarimetry in the Southern Hemisphere. Astron. Astrophys. **608**, 146 (2017). https://doi.org/10.1051/0004-6361/201731459. arXiv:2212.05985 [astro-ph.GA]
12. Versteeg, M.J.F., Magalhães, A.M., Haverkorn, M., Angarita, Y., Rodrigues, C.V., Santos-Lima, R., Kawabata, K.S.: Interstellar polarization survey. II. General interstellar medium. Astron. J. **165**(3), 87 (2023). https://doi.org/10.3847/1538-3881/aca8fd. arXiv:2212.05985 [astro-ph.GA]

13. Panopoulou, G.V., Markopoulioti, L., Bouzelou, F., Millar-Blanchaer, M.A., Tinyanont, S., Blinov, D., Pelgrims, V., Johnson, S., Skalidis, R., Soam, A.: A compilation of optical starlight polarization catalogs. Astrophys. J. Suppl. Ser. **276**(1), 15 (2025). https://doi.org/10.3847/1538-4365/ad8b21. arXiv:2307.05752 [astro-ph.GA]
14. Ichimoto, K., Lites, B., Elmore, D., Suematsu, Y., Tsuneta, S., Katsukawa, Y., Shimizu, T., Shine, R., Tarbell, T., Title, A., Kiyohara, J., Shinoda, K., Card, G., Lecinski, A., Streander, K., Nakagiri, M., Miyashita, M., Noguchi, M., Hoffmann, C., Cruz, T.: Polarization calibration of the solar optical telescope onboard hinode. Sol. Phys. **249**(2), 233–261 (2008). https://doi.org/10.1007/s11207-008-9169-9
15. Luo, J., Liu, D., Wang, B., Bi, L., Zhang, K., Liu, Y., Wen, C., Jiang, L., Yang, L., Su, L.: Effects of a nonideal half-wave plate on the gain ratio calibration measurements in polarization lidars. Appl. Opt. **56**(29), 8100 (2017). https://doi.org/10.1364/ao.56.008100
16. Savini, G., Pisano, G., Ade, P.A.R.: Achromatic half-wave plate for submillimeter instruments in cosmic microwave background astronomy: modeling and simulation. Appl. Opt. **45**(35), 8907–8915 (2006). https://doi.org/10.1364/AO.45.008907
17. Salatino, M., Bernardis, P., Masi, S.: Modeling transmission and reflection mueller matrices of dielectric half-wave plates. J. Infrared Millim. Terahertz Waves **38**(2), 215–228 (2017). https://doi.org/10.1007/s10762-016-0320-7
18. Giardiello, S., Gerbino, M., Pagano, L., Errard, J., Gruppuso, A., Ishino, H., Lattanzi, M., Natoli, P., Patanchon, G., Piacentini, F., Pisano, G.: Detailed study of HWP non-idealities and their impact on future measurements of CMB polarization anisotropies from space. Astron. Astrophys. **658**, 15 (2022). https://doi.org/10.1051/0004-6361/202141619. arXiv:2106.08031 [astro-ph.CO]
19. Collett, E.: Polarized light. Fundamentals and applications. CRC Press (1992)
20. Bird, G.R., Parrish, M. Jr.: The wire grid as a near-infrared polarizer. J. Opt. Soc. Am. (1917-1983) **50**(9), 886 (1960). https://doi.org/10.1364/JOSA.50.000886
21. Xu, M., Urbach, H.P., de Boer, D.K.G., Cornelissen, H.J.: Wire-grid diffraction gratings used as polarizing beam splitter for visible light and applied in liquid crystal on silicon. Opt. Express **13**(7), 2303 (2005). https://doi.org/10.1364/OPEX.13.002303
22. Liu, W., Yu, T., Sun, Y., Lai, Z., Liao, Q., Wang, T., Yu, L., Chen, H.: Highly efficient broadband wave plates using dispersion-engineered high-index-contrast subwavelength gratings. Phys. Rev. Appl. **11**(6), 064005 (2019). https://doi.org/10.1103/PhysRevApplied.11.064005
23. D'Alessandro, G., Mele, L., Columbro, F., Pagano, L., Piacentini, F., de Bernardis, P., Masi, S.: Systematic effects induced by half-wave plate precession into measurements of the cosmic microwave background polarization. Astron. Astrophys. **627**, 160 (2019). https://doi.org/10.1051/0004-6361/201834495. arXiv:1906.07010 [astro-ph.IM]
24. Elmore, D.: A polarization calibration technique for the advanced stokes polarimeter. NCAR Technical Notes (1990). https://doi.org/10.5065/D6959FHZ
25. Saito, T., Sutani, T., Kiyono, K., Oikawa, T.: Polarization Characterization of LEDs by Stokes Parameters Measurements. In: Journal of Physics Conference Series. Journal of Physics Conference Series, vol. 2149, p. 012009. IOP, (2022). https://doi.org/10.1088/1742-6596/2149/1/012009
26. Sheppard, R., Colin, J., Castello, M., Diaspro, A.: Three-dimensional polarization algebra. J. Opt. Soc. Am. A **33**(10), 1938 (2016). https://doi.org/10.1364/JOSAA.33.001938
27. Gell-Mann, M.: Symmetries of baryons and mesons. Phys. Rev. **125**(3), 1067–1084 (1962). https://doi.org/10.1103/PhysRev.125.1067

Authors and Affiliations

Paolo de Bernardis[1,2,3] · Silvia Masi[1,2,3] · Giulia Barbieri Ripamonti[1,3] · Fabio Columbro[1,3]

✉ Paolo de Bernardis
paolo.debernardis@roma1.infn.it

Silvia Masi
silvia.masi@roma1.infn.it

Giulia Barbieri Ripamonti
giulia.barbieriripamonti@uniroma1.it

Fabio Columbro
fabio.columbro@roma1.infn.it

[1] Physics Department, University of Rome "La Sapienza", P.le Aldo Moro 2, Roma 00185, Italy

[2] IAPS, INAF, Via del Fosso del Cavaliere 100, Roma 00133, Italy

[3] Sezione di Roma, INFN, P.le A. Moro 2, Roma 00185, Italy